

# Geomechanical behavior evolution of the rock mass involved in the Arteara rock avalanche, Gran Canaria, Canary Islands, Spain

L M Antón-Bayona<sup>1</sup>, M J Rodríguez-Peces<sup>1</sup> and J Yepes<sup>2</sup>

<sup>1</sup> University Complutense of Madrid, Spain

<sup>2</sup> University of Las Palmas de Gran Canaria, Spain

jorge.yepes@ulpgc.es

**Abstract.** In Arteara (Canary Island), a Holocene rock avalanche comprises accumulation of large reddish blocks which cover the Fataga ravine. This course, is entrenched into the Phonolitic Formation, an alternating sequence of lava flows and ignimbrites. The avalanche defines an elongated deposit of variable thickness. A low friction angle was deduced, which is related to an easily weathered bedrock favorable to the rolling of the blocks. The movement would have been a dry granular flow with a component of saltation at the head and of turbulent flow at the intermediate and distal areas. The deposit varies widely in size and is structured in bands of blocks with a polymodal distribution and low selection. The geomechanical properties of the rocks involved vary substantially in each block and along a longitudinal profile of the deposit. Schmidt Hammer rebound measured in 233 blocks show a polymodal dispersion. Some facies have been differentiated in the blocks, not only by their appearance, but also by their rebound index (R). The different hardness reflects the differences in density and porosity. The hardness zoning shows the differential weathering of the blocks, which depends on the rock anisotropy and the flow turbulence, which determines the influence of abrasion and punching of the blocks. The rebound shows a direct correlation with the bulk density and an inverse correlation with the distance to the source area.

## 1. Introduction

### 1.1. Objective

How does the alteration of a rock evolve over time? What is the law that relates the mechanical strength of a lithotype to the different degrees of weathering that it can experience? In this paper, the bases are laid to estimate the pattern that follows the mechanical alteration of two volcanic lithotypes: phonolite and non-welded ignimbrite. For this, the determination of the Schmidt Hammer rebound has been chosen. The tests were carried out in the blocks of a rock avalanche deposit.

This analysis is required to propose a relationship that follows the Barton-Bandis failure criterion and that describes the evolution of the friction angle as a function of the rebound index.

It is assumed as hypothesis that the mechanical weathering experienced by the blocks during a dry granular flow can be correlated with the effect of time on the chemical weathering process. In this way, field surveys would be reduced, because to characterize a lithotype it would not be required to



correlate the data obtained in several rock masses with different degrees of weathering. It would be enough to locate an avalanche deposit that can be sectorized in different degrees of weathering.

### 1.2. Background

There are previous works that correlate the rebound between the different Schmidt-Hammer types [1-2] in the field and with respect to other laboratory tests (uniaxial compressive strength, Young's modulus, etc.) in a geological-geotechnical context [3-17]. This approach has also been applied in volcanic territories, but less frequently [18-21].

In civil engineering, the Schmidt-Hammer has been used to evaluate the quality of construction materials [22-23] and the excavability of the rock massif [24-25].

The use of the Schmidt-Hammer for the relative dating of rock avalanches has a long tradition. These works relate the exposure of an outcrop with the alteration of the rock, based on the surface hardness of the material. Most of the contributions have been collected in reviews [26-30].

The combined use of the Schmidt-Hammer with the analysis of exposure to cosmogenics has increased the reliability of the proposed chronological sequences in igneous massifs. The work carried out on volcanic rocks has experienced a resurgence due to the use of chlorine [31] and Helium isotopes [32].

This work aims to characterize the geomechanical properties of volcanic materials involved in a large rock avalanche, following the methodology of previous authors [33-42]. The results obtained will be correlated with the ages of exposure to cosmogenics and the detachment of the initial block and the flow of the avalanche will be modeled.

### 1.3. Context

The present study is located in Arteara (figure 1), a ravine in Gran Canaria (Canary Islands), where a very recent-looking rock avalanche deposit (figure 2) covers a steep slope of the Fataga ravine, embedded about 600m in a monotonous series in which phonolitic and ignimbritic lava flows alternate. Two materials with a very different rheological behavior. Phonolite is more dense, massive and resistant to compression than ignimbrite. The avalanche deposit covers a previously slipped rock mass and is partially covered at the headwaters by a sequence of active scree (figure 3).

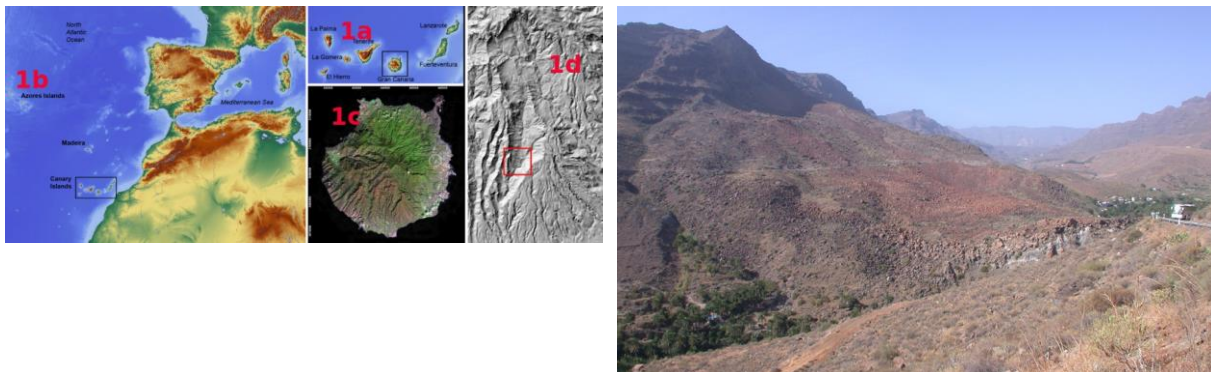


**Figure 1.** Location of the study area. (b) Canary Islands. (a and c) Gran Canaria. (d) Arteara rock avalanche in the Fataga ravine.

**Figure 2.** The rock avalanche of Arteara seen from the South, lining the right side of the Fataga ravine.

The study focuses on the analysis of the rebound index measured in a population of 233 blocks selected from among the 471 inventoried elements (Table 1; figure 4) that are part of the deposit of a rock avalanche that has a longitudinal development of about 1500 m, which extends over an area of about 0.565 km<sup>2</sup> and has an estimated volume of about 12203055 m<sup>3</sup> to 6101527 m<sup>3</sup>, depending on a thickness of 10 m or 5 m, respectively [43-45].

**Table 1.** Distribution of the blocks tested according to geomorphological sectors, morphometric classes and differentiated lithotypes. Note: Headland scarp data has been omitted because the rebound was measured directly on the rocky outcrop.

<i>Sector</i>	<i>Lithotype</i>	<i>Volume (m<sup>3</sup>)</i>				<i>Partial</i>	<i>Total</i>
		0-27	27-64	64-125	>125		
<b>Scree</b>	Phonolite (P)	3	11	0	0	14	14
	Non-welded ignimbrite (NWI)	0	0	0	0	0	
	welded ignimbrite (WI)	0	0	0	0	0	
<b>Top Area</b>	Phonolite (P)	4	7	0	0	11	17
	Non-welded ignimbrite (NWI)	0	3	1	0	4	
	welded ignimbrite (WI)	0	2	0	0	2	
<b>Middle Area</b>	Phonolite (P)	5	14	3	0	22	35
	Non-welded ignimbrite (NWI)	1	5	1	2	9	
	welded ignimbrite (WI)	0	3	0	1	4	
<b>Distal Area</b>	Phonolite (P)	58	18	20	21	117	167
	Non-welded ignimbrite (NWI)	17	20	8	4	49	
	welded ignimbrite (WI)	1	0	0	0	1	
<b>TOTAL</b>		89	83	33	28	233	233

The proposed objective is to determine whether the deduced low friction angle ( $\Phi = 21^\circ$ ) previously estimated [43] and the high longitudinal development that it presents is related to the existence of a previous slope favorable to the bearing of the blocks and to the lubricating action of the non-welded ignimbrites [43-45] or, it requires an initial speed of the fall of the initial block that was related to a Holocene earthquake-volcanic crisis.

To solve the question raised, a geotechnical approach has been proposed: evaluate the spatial distribution of the rebound index obtained with the Schmidt Hammer, along the longitudinal axis of the deposit. A 2D type profile.

Geomorphological observations made in previous studies [43-45] have allowed us to suppose that the movement of the blocks would have been a dry granular flow with a saltation component at the head and turbulent flow in the middle and middle areas. distal.

The criterion followed in the choice of the tested blocks has tried to include the different typologies identified in the set by the previous studies, both lithological [46-49], as well as morphometric and geomorphological.

From the lithological point of view, it has been ensured that the largest number of lithotypes identified in the vicinity (phonolite, non-welded ignimbrite, welded ignimbrite and non-welded and hydrothermally altered ignimbrite) by the previous phases of this work were present [46-49], although the most abundant sample corresponds to the phonolite and non-welded ignimbrite classes (figure 4).

Regarding morphometry, size blocks corresponding to the different classes identified in the 1m / pix precision orthophoto (0-8m<sup>3</sup>; 8-27m<sup>3</sup>; 27-64m<sup>3</sup>; 64-125m<sup>3</sup>) have been sampled.

With regard to geomorphology, data have been collected from the five areas in which the deposit has been sectorized (Head Escarpment, Canchal, Upper Landing, Middle Section and Distal Area).

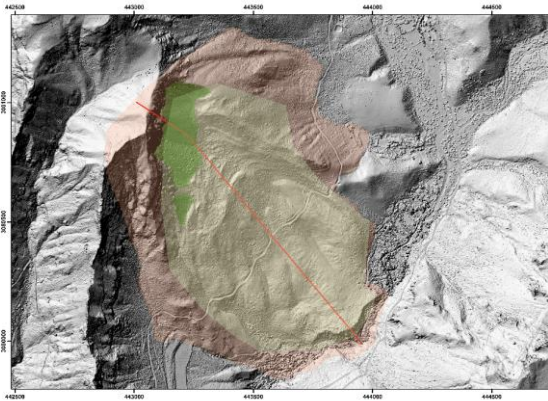


**Figure 3.** The rock avalanche (yellow) covers a previous translational rock slide (red) and is partially covered at the head by a sequence of active scree (green). The longitudinal axis on which the R measured with the Schmidt Hammer has been projected is indicated in red.

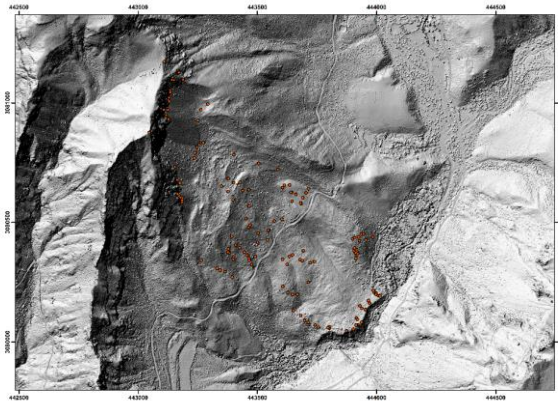


**Figure 4.** Location of the 233 blocks included in the rock avalanche that have been tested with the Schmidt Hammer.

## 2. Results

### 2.1. The rebound index in the total set of blocks

The average data obtained in each of the tests carried out (figure 5) shows a certain inverse correlation between the value of the rebound index and the distance to the source area.

From the headland scarp to the foot, the reduction in average hardness is accompanied by a decrease in both the range between the maximum and minimum average values, as well as the maximum average value. The maximum-minimum difference varies between 55 at the head and 25 at the foot and the maximum values of the average decrease from 75 to 45.

However, the distribution of the standard deviation (figure 6) shows a slight contraction in the middle section. Both the headland and footing values range between 17 and 7, while in the middle section, at around 500-1000m, a slight concentration of Ds is observed around 10.

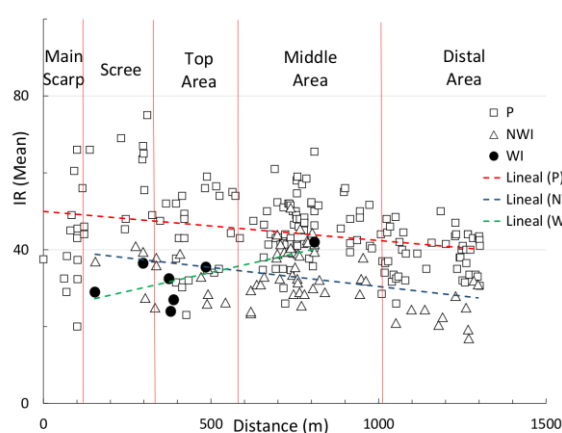


**Figure 5.** Distribution of the average values of R measured with the Schmidt Hammer in the avalanche blocks sampled.

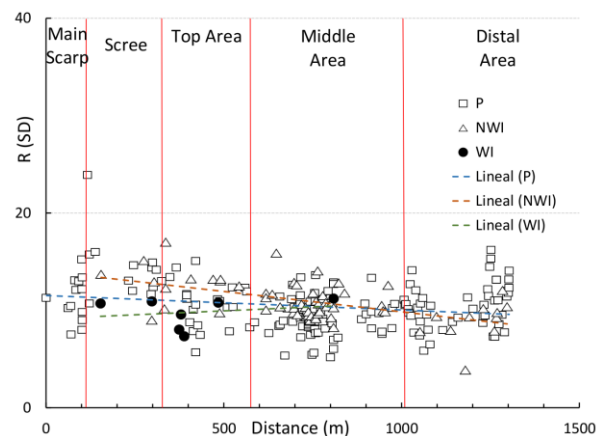


**Figure 6.** Distribution of the standard deviation values estimated from the R values measured in the avalanche blocks sampled.

## 2.2. The rebound index in the phonolite blocks

The quote graph generated with the data from the phonolite blocks (figure 7) shows, on the one hand, the fluctuations experienced by the range between the maximum and minimum values of the average throughout the deposit and, on the other hand, shows the decrease in the range itself as the blocks are further from the source area. Fluctuations are observed randomly within each of the 5 differentiated geomorphological units. For its part, the reduction of the absolute value of the maximum-minimum range is more evident in the distal area, where the values go from moving between 100 and 10 to being limited within the 60-20 range.

The sectorial analysis of R measured in the phonolite blocks (figure 8) shows a complex distribution pattern for the hard lithotype (phon). In general, the average value of the rebound index increases with the distance to the escarpment, within each of the proximal sectors (escarpment, scree and headland landing), while it remains constant in the middle and distal sectors.

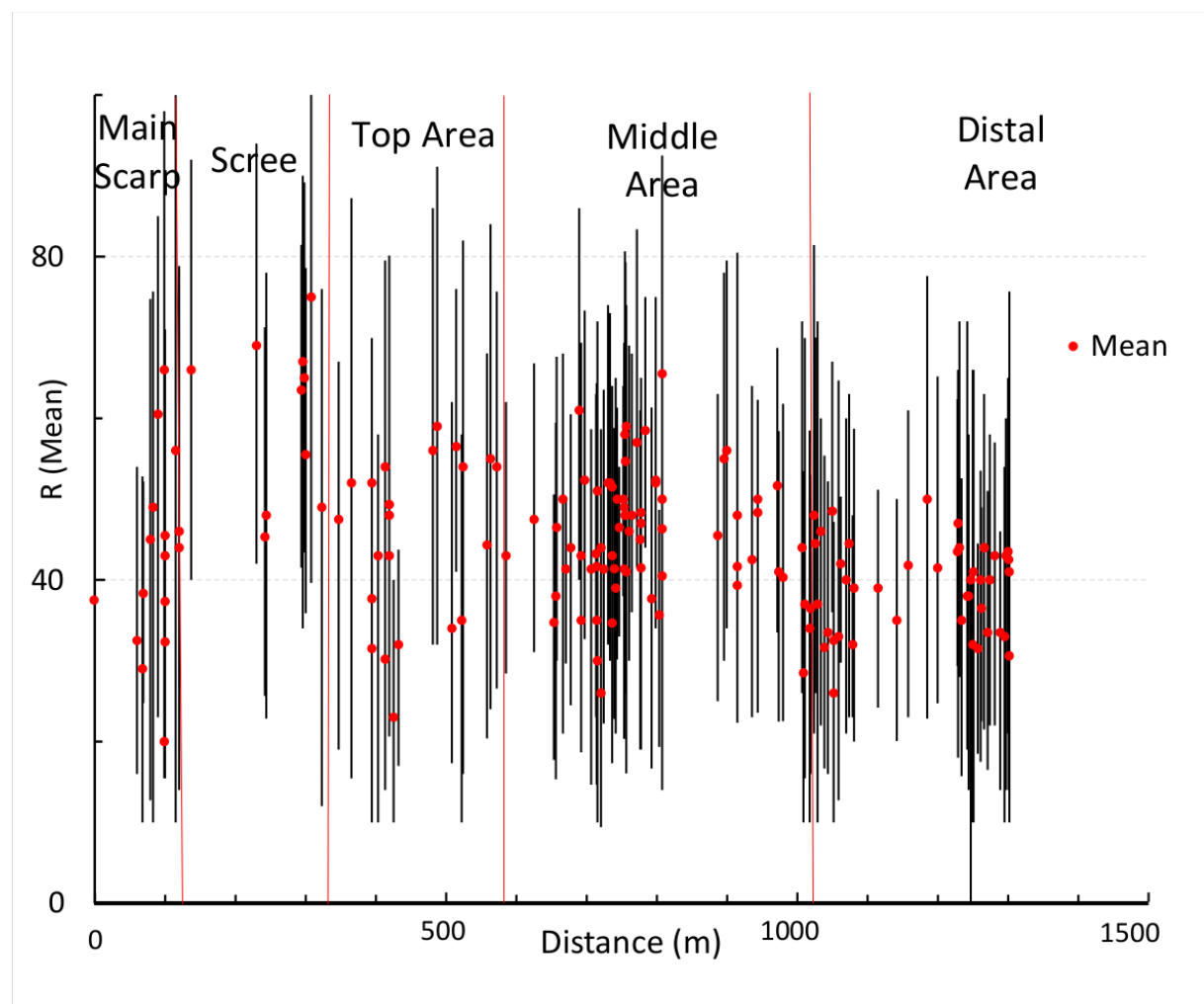


**Figure 7.** Quote graph generated from the averages and the maximum and minimum values of R measured in the sampled phonolite blocks.

The standard deviation recorded in phonolite (Fig 9) and non-welded ignimbrite (fig. 14) is similar and oscillates in a range of 5-15. Although the minimum value of the deviation corresponds to the phonolite

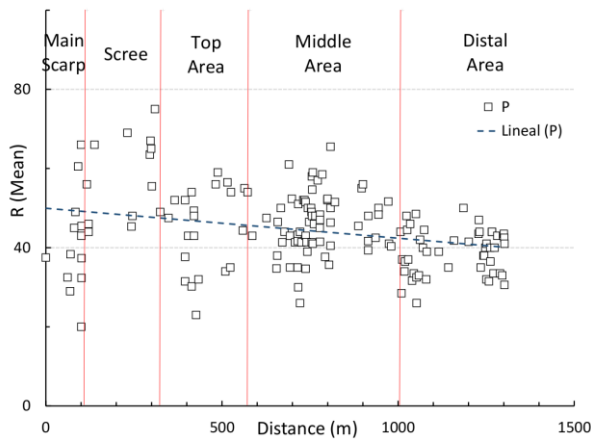


**Figure 8.** Average values of the phonolite blocks calculated from the R measured in the avalanche blocks sampled.

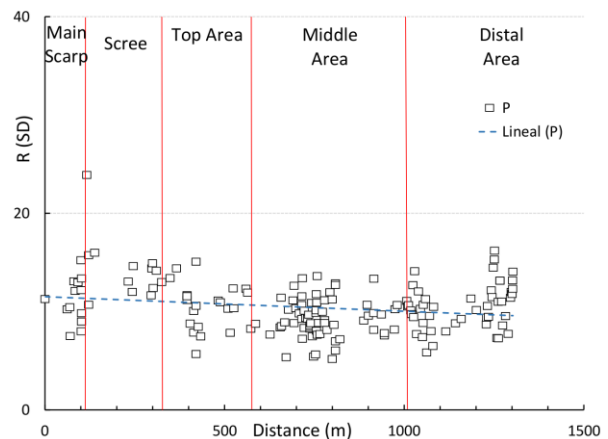


**Figure 9.** Values of the estimated standard deviation in the phonolite blocks from the R measured in the sampled avalanche blocks.

The sector-by-sector of R measured in the phonolitic rock cloths with a massive texture (core facies) shows a complex distribution pattern (fig. 10). the pattern is similar to that observed with the averages of all the tests performed on the phonolites. It even seems that the effect is amplified. The average value of R increases within each sector as it separates from the escarpment (Main Scarp, Scree, Top Area, etc.). Although it is true that both the average R, and its increase, is less with increasing distance to the escarpment.

The statistical distribution of R in the phonolite blocks (figure 11) shows the existence of several modal intervals. The graphical analysis by sectors was carried out taking as a sample all the tests carried out on the phonolites. The pattern of the distribution is similar to that of the average values. Within each sector of the avalanche, the adjustment functions have a direct correlation with the distance to the main scarp. However, in general terms both the absolute value of the mode and its increase decrease as the distance from the escarpment increases.

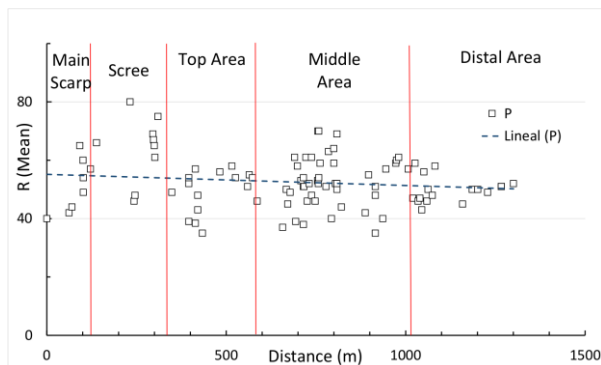


**Figure 10.** Average values of R measured in the differentiated nucleus facies in the sampled phonolite blocks.

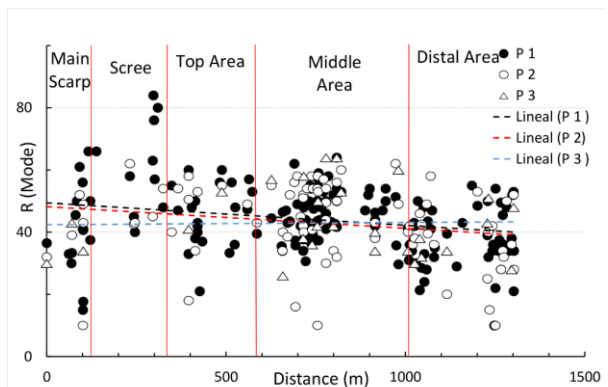


**Figure 11.** Values of the principal modes estimated in the phonolite blocks from the R measured in the sampled avalanche blocks.

### 2.3. The rebound index in the welded phonolite blocks

As in the case of the phonolites, the price graph of the non-welded ignimbrites (figure 12) shows, on the one hand, the fluctuations experienced by the range between the maximum and minimum values of the average throughout the deposit and on the other hand In part, it shows the decrease in the range itself as the blocks are further away from the source area.

Also in this lithotype, random fluctuations are observed within each of the 5 differentiated geomorphological units. Furthermore, the reduction of the absolute value of the maximum-minimum range is more evident in the distal area, where the values go from moving between 70 and 10 to being limited within the 50-10 range. However, the fluctuations offered by the non-welded ignimbrite stock chart are more attenuated than in the phonolites.

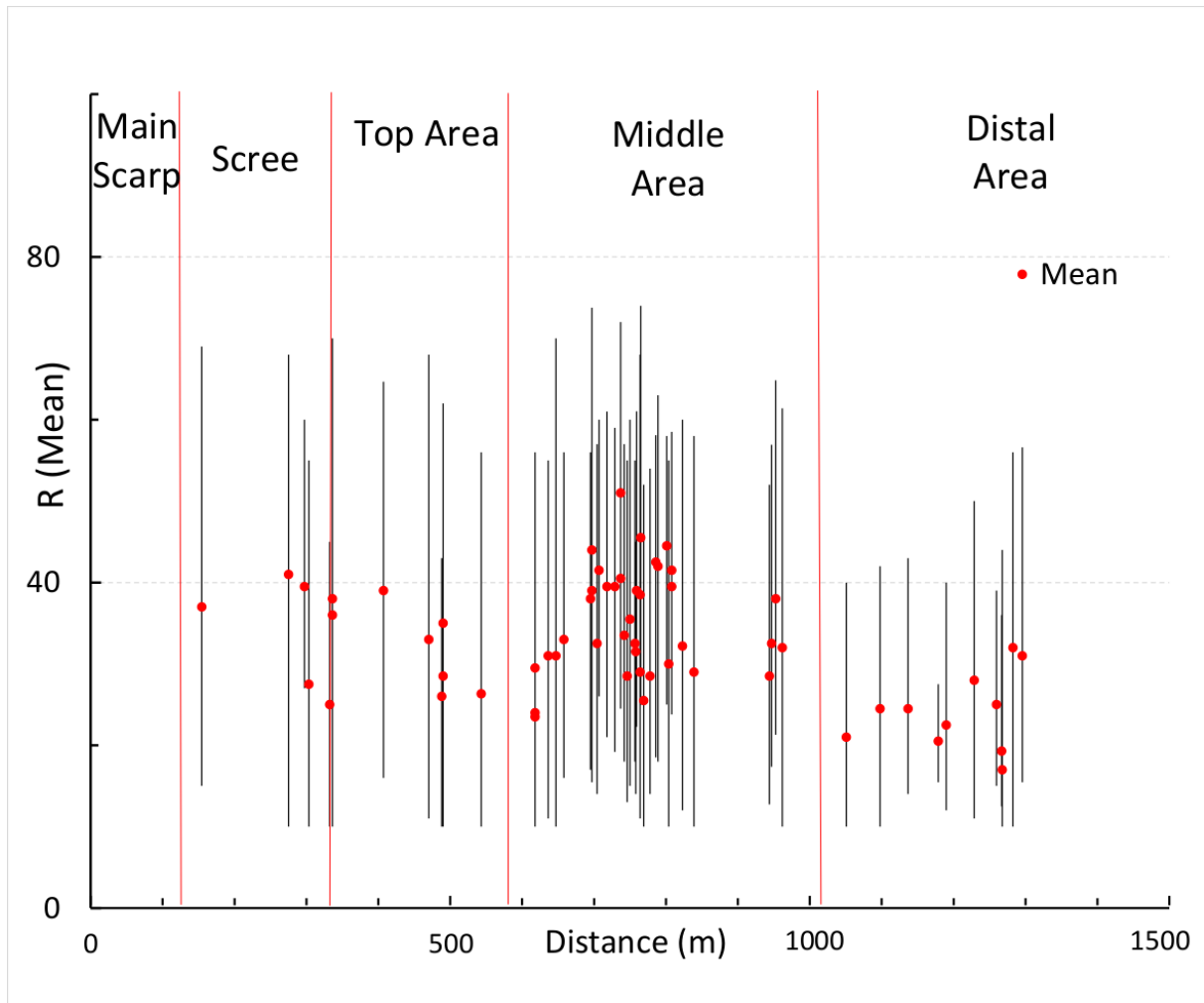


**Figure 12.** Quotation graph generated from the averages and the maximum and minimum values of R measured in the non-welded ignimbrite blocks sampled.

The graphical distribution of the average R values measured in the non-welded Ignimbrites (figure 13) shows a variable trend and a poor correlation with the distance to the main scarp. In general terms, a slight inverse R-Distance correlation is observed, however a rebound in surface hardness is observed in the blocks of the middle section that have been sampled.

In any case, the averages recorded oscillate in a range of values (20-50) much lower than that of the phonolite blocks.

As already mentioned, the standard deviation recorded in phonolites (figure 9) and non-welded ignimbrite (figure 14) is similar and ranges from 5-15. Although the minimum value of the deviation corresponds to the phonolites.

In general terms, the standard deviation in the ignimbritic lithotype (figure 14) decreases along the deposit, moving away from the main escarpment. The behavior of the blocks located in the distal area would be an exception. At the edge of the foot there is a slight upturn in dispersion.

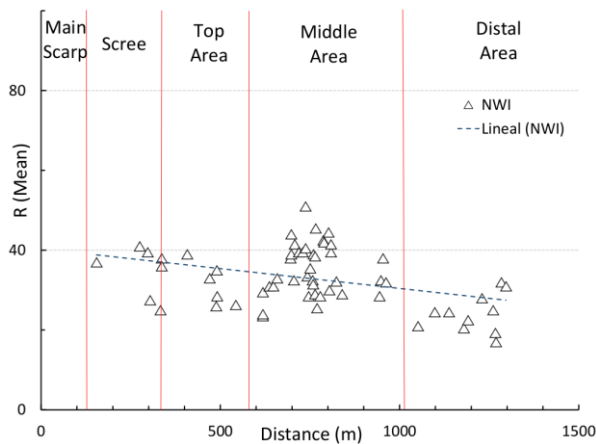


**Figure 13.** Average values of non-welded ignimbrite blocks calculated from R measured in the avalanche blocks sampled.

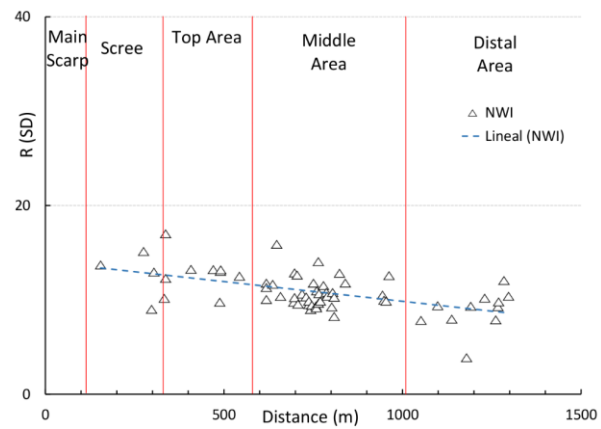


**Figure 14.** Values of the estimated standard deviation in the non-welded ignimbrite blocks from the R measured in the sampled avalanche blocks.

The graphical distribution of R in the block facies (skeleton) of the ignimbrites (figure 15) shows a trend similar to that observed when analyzing the entire non-welded ignimbrite block. However, the averages recorded oscillate in a wider range of values (20-60), although it is still lower than that of the phonolite blocks.

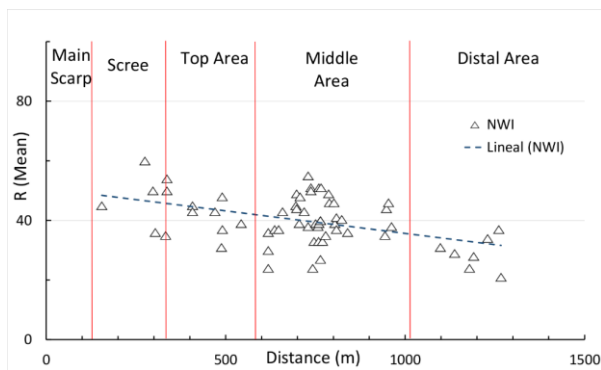


**Figure 15.** Average values of non-welded ignimbrite blocks (skeleton facies) calculated from R measured in the avalanche blocks sampled.

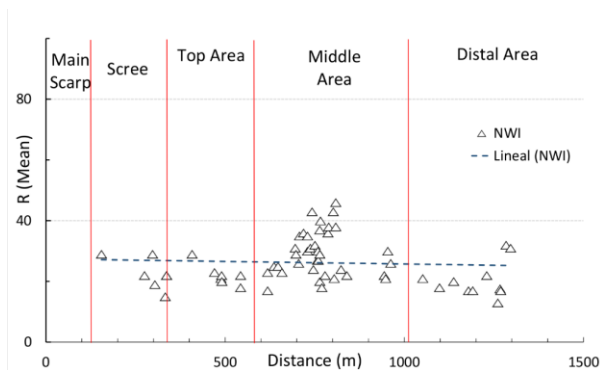


**Figure 16.** Average values of non-welded ignimbrite blocks (matrix facies) calculated from R measured in the avalanche blocks sampled.

The rebound values measured in the non-welded ignimbrite matrix facies (figure 16) offer variable trends and a low fit. A behavior similar to that shown by the total data of each block.

However, the averages recorded in the matrix oscillate in a higher range of values (15-45) than that presented by the blocks considered as a whole.

The statistical distribution of R shows the existence of several modal intervals in the non-welded ignimbrite lithotype (figure 17), as in the case of phonolite (figure 11). The graphical analysis by sectors was carried out taking as a sample all the tests carried out in the non-welded ignimbrite blocks. The pattern of the distribution is highly variable. More than in the case of the phonolite. Within each sector of the avalanche, the adjustment functions have a direct poor correlation with the distance to the

main scarp. However, in general terms, both the absolute value of the mode and its range or fluctuation decrease with increasing distance from the escarpment.

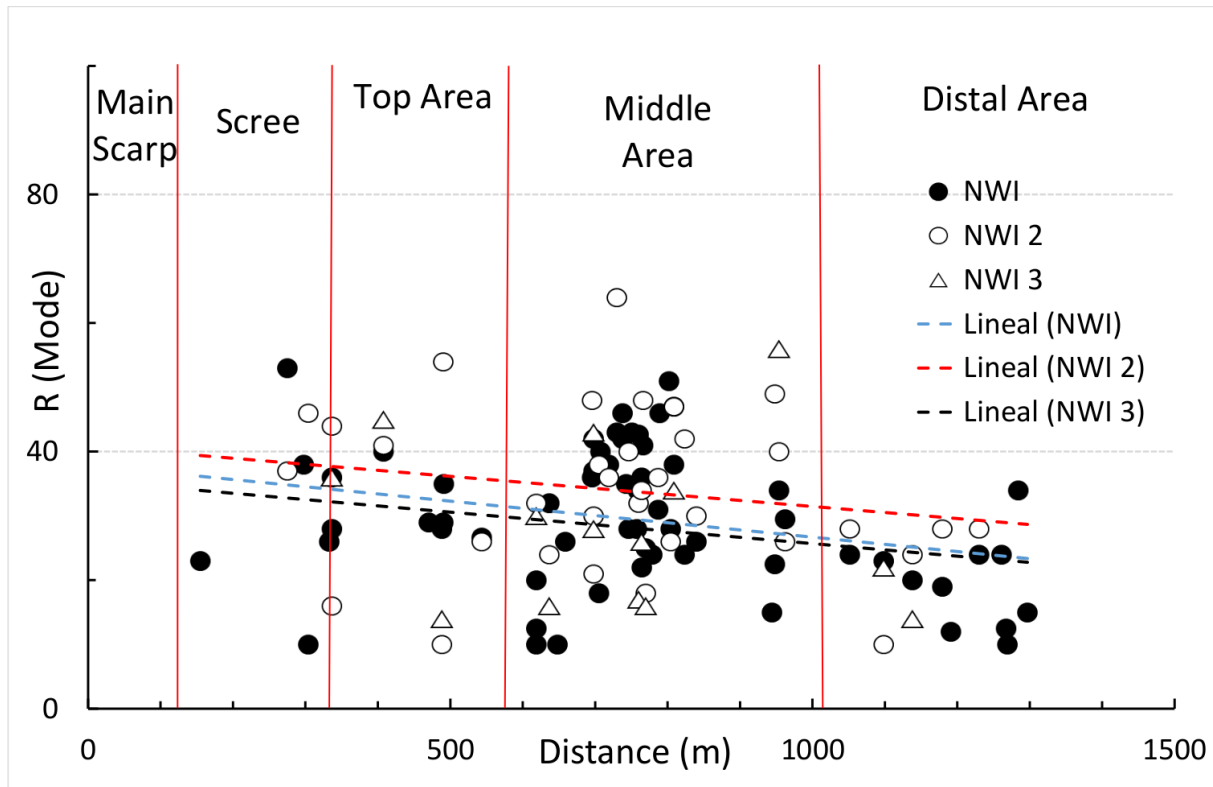


**Figure 17.** Values of the principal modes estimated in the non-welded ignimbrite blocks from the R measured in the sampled avalanche blocks.

Two other rare lithotypes have been identified in the avalanche deposit from visual observations. One welded ignimbrite and one non-welded and hydrothermally altered ignimbrite. The small number of sampled blocks does not allow to propose consistent hypotheses in relation to their rheological behavior. However, in a first approximation, some observations are offered.

In global terms, the graphical fit of the average values calculated for the welded ignimbrite blocks shows a constant trend with increasing distance to the main scarp. The fit is poor, the trend falls within a moderate range of values (20-40) and the standard deviation is small (approx 10).

### 3. Discussion

#### 3.1. The rebound index in the total set of blocks

The reduction in surface hardness with stopping distance is consistent with the increase in blows and friction between blocks typical of the dry flow process that characterizes rock avalanches (figure 5).

The decrease in both the range between the values of the maximum and minimum averages, as well as the maximum value of the average is consistent with the idea that the transport process manages to homogenize the geomechanical characteristics of the material, for example: hardness and size (figure 5).

The reduction of the deviation in the intermediate section corroborates the ideas pointed out when analyzing the data of the mean values (figure 6).

### 3.2. *The rebound index in the phonolite blocks*

The fluctuations in the range offered by the stock chart (figure 7) are consistent with the assumption that several events have occurred in time and that their deposits are overlapping in space.

Small values of R in the main escarpment would be related to two different factors. On the one hand, with the advanced state of chemical weathering in which the upper erosion surface is found, whose antiquity dates back to at least 9 Ma. And, on the other hand, with the intense mechanical weathering that affects the main escarpment in the sectors where the massif is highly compartmentalized by a network of open cracks that have arisen in the back of the main fracture that triggered the rock avalanche (figure 7).

Just as the distribution graph of the average values of R shows an inverse correlation with distance, in the case of the stock graph (figure 7) a decrease in the range between the values of the maximum and minimum averages is clearly observed. In the distal area, as well as its homogenization, at least in the distal area. The low values of R in the distal area are consistent with the higher degree of mechanical weathering that the blocks transported a greater distance withstand, as well as with the idea that the transport process manages to homogenize the geomechanical characteristics of the transported material, for example: the hardness and size.

The wide ranges between the values of the maximum and minimum averages observed in the headwater escarpment (figure 7) are related to the fact that the sampled phonolytic lava blocks and outcrops offer several textural facies with different degrees of alteration: the jointed, altered, flaked facies and the core facies.

The jointed facies corresponds to the sector of a block that presents the discontinuities between lava flows opened by an energetic impact received during a flow in which saltation transport would predominate.

The altered facies corresponds to the sector of the block that has been affected by mechanical grinding caused by friction between blocks during the dry flow of the avalanche. The energy of this flow would be less than that assumed for the jointed facies and could be attributed to a laminar flow in which rolling transport would predominate. This facies gives the surface of the blocks a homogeneous appearance, without discontinuities, which is usually partially covered by a tapestry of bryophytes.

The scale facies corresponds to the sectors in which the chemical weathering process has penetrated the rock enough to define several layers with different degrees of cohesion, which determines the appearance of a joint parallel to the surface of the block in favor from which the crust of the block is peeled.

The core facies offers the highest R values. This facies corresponds to the healthy heart of a rock that is exposed by the breakage of a rock chip or wedge, the consequence of a high-energy impact.

The information transmitted by the R analysis by sectors shows a complex pattern for the phonolite lithotype (figure 8). In general terms, it seems that by increasing the route made by the blocks, their homogenization increases. The increase in R within the proximal sectors suggests several hypotheses. The first, that there would have been several events of different energy that would have happened in time. The most energetic events would have determined the greater reach of the blocks (middle and distal sectors). The less energetic events would be related to most of the blocks located in the proximal sectors. It seems logical to assume that the oldest events would have been the most energetic. This makes it possible to recognize more modern and less energetic deposits by partially covering older and energetic event deposits. The opposite would be impossible. The second hypothesis is that the oldest events correspond to episodes related to a rocky block of greater dimensions or related to earthquake-volcanic activity. In both cases the total starting energy would be greater and, consequently, the distance reached by the blocks. Third, it seems logical to think that, after a highly energetic event, such as a rock avalanche, lower-energy events will occur that release the residual stresses of the massif. These events would have resulted in episodic landslides and scree sequences and would be like an echo of the original event.

On the other hand, the moderate dispersion of R (standard deviation, figure 9) estimated in the phonolite blocks suggests the recent character of the deposit. The weathering process does not appear

to have advanced significantly. In fact, the most significant dispersion is located in the main escarpment, where fresh and healthy rock layers coexist with highly fragmented rock wedges.

Furthermore, the amplified response offered by the graph of the core facies (figure 10) corroborates the hypothesis that the dry granular flow only affects the surface crust of the blocks, which behave like the aggregates in the Los Angeles test or in the Microdeval assay.

Finally, the existence of up to three main modes in the analyzed sample (figure 11) corroborates the hypothesis that phonolite blocks present several textural facies. These facies express the differential alteration experienced by the blocks involved in the dry granular flow. An alteration that mainly affects the surface layer (jointed, altered, flaking facies) and, to a lesser extent, its interior (core facies).

This observation makes it possible to propose a variation of the internal friction angle of the materials involved, depending on the tendency shown by the rebound measured with the Schmidt Hammer. This will be done by applying the Barton failure criterion. All these previous analyzes will facilitate the estimation of the pattern of mechanical alteration experienced by the different lithotypes involved in the flow process.

### *3.3. The rebound index in the non-welded phonolite blocks*

The interpretation of the stock chart (figures 7 and 12) is similar in both lithotypes. The fact that the range fluctuations are attenuated in the non-welded ignimbrite (figure 12) suggests the homogenizing character of the matrix facies, whose surface hardness oscillates in a similar range throughout the entire deposit (0-25).

Non-welded ignimbrite blocks are composed of particles of different size and composition that are welded together at high temperatures. The abundance of one or the other size makes it possible to differentiate three facies: the matrix facies, characterized by the exclusive presence of particles with a size between millimeter and centimeter. The skeletal facies, represented by particles of intermediate size (decimetric order). Finally, there would be the fragment facies, which would be represented by fragments of lava of decimeter to metric order. In general, the skeletal facies is usually enveloped by the matrix facies and defines a sustained matrix texture. It is not common to identify grainy-tended facies in which skeletal clasts predominate.

The low values reached by the average R in the non-welded ignimbrite (figure 13) is related to the low surface hardness of the matrix. This facies lowers the global average of the blocks.

On the other hand, the clear downward trend offered by the average R values seems consistent with the increase in the distance to the main escarpment (figure 13). The upturn in hardness observed in the intermediate section, 700-900m from the main escarpment, requires a particular analysis.

The slight increase in R in the distal area could be attributed to the fact that these blocks have hardly been impacted by other blocks that experienced saltation transport. On the other hand, in the proximal sector (scree and head landing), many blocks are observed with notches from high energy impacts and, in some cases, chipped and partially covered by splinters from the impact block (figure 13).

The moderate value of the dispersion (figure 14) corroborates the recent nature of the deposit. The rebound in the standard deviation observed in the foot could be attributed to the fact that this lithotype has the behavior of a soft rock with a certain capacity to absorb deformations in the plastic range, which allows us to suppose that its reaction to roughing or Faced with punching, it would have given rise to an advanced state of microfracturing that would determine the dispersion of the rebound in the same block, depending on whether the test is performed on the matrix facies or on the block facies.

The amplified response offered by the graph of the block facies (figure 15) corroborates the hypothesis that the non-welded ignimbrite macro-factory is heterogeneous and that it can be assimilated to that of a sedimentary gap made up of two fractions of different sizes: a skeleton of Coarse and angular clasts enveloped and pasted by a detrital matrix made up of granular material with a particle size one or two orders of magnitude smaller than the clasts of the skeleton.

The slight differences observed in the mechanical response offered by the non-welded ignimbrite blocks (figure 13) and the skeletal facies (figure 15) could be attributed to the structural variability of the material. non-welded ignimbrite is the result of mixing, in highly variable proportions, elements with different porosity and degree of welding.

The variability of the trends and the low adjustment of the rebound data (figure 13), together with moderate but constant standard deviation values throughout the entire deposit (figure 14), corroborate the hypothesis that non-welded ignimbrite is a lithotype with variable rheological behavior, which is conditioned by a heterogeneous macro-factory.

The low values of surface hardness recorded in the non-welded ignimbrite matrix (figure 16) are consistent with the existence of intergranular porosity that does not exist in the skeletal facies and that supposes a decrease in overall density and an increase of the plasticity of the material. This plasticity would be the determining factor to consider the non-welded ignimbrite lithotype as a soft rock.

The high porosity of the non-welded ignimbrite matrix determines its alterability. This fact, together with its plasticity, suggests the possibility that the ignimbritic lithotype has behaved like a carpet that reduced friction in the basal plane of the rock avalanche, conditioning the efficiency of the dry granular flow.

The existence of up to three main modes in the analyzed sample (figure 17) corroborates the hypothesis that the non-welded ignimbrite blocks present several textural facies. Skeleton and matrix would be the main ones.

The poor correlation between the rebound index (figure 13) and the distance to the source area would corroborate the idea that the variable rheological behavior is conditioned by a heterogeneous macro-factory.

#### 3.4. The rebound index in the welded phonolite blocks

Although the differentiation of lithotypes was made based on visual observation, the results of the surface hardness would allow us to compare the hardness of the welded ignimbrite sampled in Arterea with the response offered by the matrix of a non-welded ignimbrite. This result is contrary to what might be expected. In fact, in other samplings carried out previously, the resistance of the welded ignimbrite is much higher than that of the non-welded ignimbrite.

On the other hand, the low value of the standard deviation suggests that the two facies of the lithotype (matrix and skeleton) present a more homogeneous behavior than the non-welded ignimbrite. This fact is consistent with the data obtained in other outcrops.

The causes of this unforeseen behavior are not entirely clear at the moment.

## 4. Conclusion

In the main escarpment the highest and lowest values of the R are recorded. It is a sector in which weathered rock outcrops intermingle (top of the escarpment, partially slipped rock wedges) and healthy rock outcrops (fresh rock cloths that have been uncovered in recent times by the effect of landslides of large rocky blocks)

Large blocks of healthy rock of the main lithotypes (phonolite, non-welded ignimbrite) are identified in the scree that covers the headwaters. In both cases, the highest values of R have been recorded. They are the blocks detached in recent times and come from the fragments of healthy rock that were partially detached from the main escarpment after the last major avalanche recorded in this sector. This last event uncovered the heart of the massif, an area that had not been able to reach the weathering of the rock.

The middle section offers a wide range of values, with R averages ranging between 20 and 60. In addition, it presents an anomaly around the point located 800-900m from the foot of the escarpment.

In general terms, the R of the phonolite is much higher than that of the non-welded ignimbrite. The low resistance of the non-welded ignimbrite matrix greatly reduces the average rebound recorded in this lithotype.

In the case of the phonolite, there is a notable difference between the behavior offered by the core of the blocks and the average of the block as a whole. This difference allows the blocks to be zoned in concentric caps and assumes that the flow of the avalanche by jumping and rolling only efficiently affects the outer cap. These two types of movement would be conditioning the appearance of stresses that would determine the mechanical weathering of the block. On this disaggregation of the material, the biogeochemical weathering conditioned by the bryophyte mantles that colonize the surface of the blocks and partially cover them would advance with greater efficiency. The saltation process would be related to the punching pressure, while the rolling process would be conditioning the surface roughing.

Finally, there seems to be an inverse correlation between the block size and the range of the recorded values, at least in the phonolite lithotype. In fact, phonolite blocks that have a size between 0.5 and 1m<sup>3</sup> usually offer very high and homogeneous R values. This observation would be related to the fact that the reduction of the block size by successive breaks also reduces the variability of possible facies in the same block. Thus, the core facies would give rise to massive blocks of metric to decimeter order, while the rest of the facies would give rise to centimeter-sized gravels, for which there is no data.

## References

- [1] Basu A, Aydin A 2004 A method for normalization of Schmidt hammer rebound values. *International Journal of Rock Mechanics & Mining Science* 41 1211–1214. DOI:10.1016/j.ijrmms.2004.05.001
- [2] Ayday C, Goktan R M 1992 Correlation between N-type and L-type Schmidt hammer rebound values obtaining during field testing. *Eurock'92*: 47-50. Thomas Telford. London
- [3] Day M J, Goudie A S 1977 Field assessment of rock hardness using the Schmidt test hammer. *British Geomorphological Research Group Technical Bulletin* 18 19-29
- [4] Hamry K Y, De Marco M J 1985 Use of Schmidt hammer for rock and coal testing. *Proc. 26 US Symp. on Rock Mech.*: 549-555. Balkema.
- [5] Evans D J A, Archer S, Wilson D J H 1999 A comparison of the lichenometric and Schmidt hammer dating techniques based on data from the proglacial areas of some Icelandic glaciers. *Quaternary Science Reviews* 18 13-41.
- [6] Kahraman S 2001 Evaluation of simple methods for assessing the uniaxial compressive strength of rock. *International Journal of Rock Mechanics and Mining Sciences* 38 9819–9894
- [7] Hack H R G K, Huisman M 2002 Estimating the intact rock strength of a rock mass by simple means. *Proceedings of the 9th congress of the International Association for Engineering Geology and the Environment*: 1971-1977
- [8] Yilmaz I, Sendir H 2002 Correlation of Schmidt hardness with unconfined compressive strength and Young's modulus in gypsum from Sivas (Turkey). *Engineering Geology* 66 211–219
- [9] Sendir H 2002 Correlation of Schmidt hardness with unconfined compressive strength and Young's modulus in gypsum from Sivas (Turkey). *Engineering Geology* 66 211–219
- [10] Karakus M, Kumral M, Kilic O 2005 Predicting elastic properties of intact rocks from index tests using multiple regression modelling. *International Journal of Rock Mechanics and Mining Sciences* 42 323-330
- [11] Aydin A 2008 ISRM suggested method for determination of the Schmidt hammer rebound hardness: Revised version. *International Journal of Rock Mechanics & Mining Sciences* 46 627–634. DOI:10.1016/j.ijrmms.2008.01.020
- [12] Aydin A, Basu A 2005 The Schmidt hammer in rock material characterization. *Engineering Geology* 81 1-14. DOI:10.1016/j.enggeo.2005.06.006
- [13] Shalabi F I, Cording E J, Al-Hattamleh O H 2007 Estimation of rock engineering properties using hardness tests. *Engineering Geology* 90 138–147
- [14] Gupta V, Sharma R, Sah M P 2009 An evaluation of surface hardness of natural and modified rocks using Schmidt hammer: study from northwestern Himalaya, India. *Geografiska Annaler* 91A 179-188

- [15] Yagiz S 2009 Predicting uniaxial compressive strength, modulus of elasticity and index properties of rocks using the Schmidt hammer. *Bulletin of Engineering Geology and Environment* 68 55-63
- [16] Viles H, Goudie A, Grab S, Lalley J 2011. The use of the Schmidt Hammer and Equotip for rock hardness assessment in geomorphology and heritage science: a comparative analysis. *Earth Surface Processes and Landforms* 36 320–333
- [17] Sharma P K, Khandelwal M, Singh T N 2011 A correlation between Schmidt hammer rebound numbers with impact strength index, slake durability index and P-wave velocity. *International Journal of Earth Sciences* 100 189-195 DOI: 10.1007/s00531-009-0506-5.
- [18] Aggitalis G, Alivizatos S, Stamoulis D, Stournaras G 1996 Correlating uniaxial compressive strength with Schmidt hardness, point load index, Young's Modulus, and mineralogy of gabbros and basalts (northern Greece). *Bulletin of the International Association of Engineering Geology* 54 3–11
- [19] Sumner P, Nel W 2002 The effect of moisture on Schmidt hammer rebound: Test on rock samples from Marion island and South Africa. *Earth Surface Process and Landforms* 27 1137-1142
- [20] Dinçer I, Acar A, Cobangulu I, Uras Y 2004 Correlation between Schmidt hardness, uniaxial compressive strength and Young's modulus for andesites, basalts and tuffs. *Bulletin of Engineering Geology and the Environment* 63 141–148
- [21] Aoki H, Matsukura Y 2004 Relationship between the equotip rebound value and unconfined compressive strength of intact rock sample. *Transactions, Japanese Geomorphological Union* 25 267-276
- [22] Aydin F, Saribiyik M 2010 Correlation between Schmidt Hammer and destructive compressions testing for concretes in existing buildings. *Scientific Research and Essays* 5 13 1644-1648
- [23] García-González C, Yepes J, Franesqui M A 2020 Geomechanical characterization of volcanic aggregates for paving construction applications and correlation with the rock properties. *Transportation Geotechnics* 24 100383
- [24] Vellone D A, Merguerian C 2007 Measuring Engineering Properties of NYC Rocks using a Schmidt Rebound Hammer Preliminary Results. in Hanson, G. N., chm., Fourteenth Annual Conference on Geology of Long Island and Metropolitan New York, 14 April 2007, State University of New York at Stony Brook, NY, Long Island Geologists Program with Abstracts, 7 p.
- [25] Goktan R M, Gunes N 2005 A comparative study of Schmidt hammer testing procedures with reference to rock cutting machine performance prediction. *International Journal of Rock Mechanics and Mining Sciences* 42 466–72
- [26] Matsukura Y, Aoki H 2004 The Schmidt hammer: a brief review and some problems in geomorphology. *Transactions of the Japanese Geomorphological Union* 25 175-196
- [27] Goudie A S 2006 The Schmidt Hammer in geomorphological research. *Progress in Physical Geography* 30 6 703-718. DOI: 10.1177/0309133306071954
- [28] Moses C, Robinson D, Barlow J 2016 Methods for measuring rock surface weathering and erosion: A critical review. *Earth-Science Reviews* 135 141-161. DOI: 10.1016/j.earscirev.2014.04.006
- [29] Viles H 2016 Technology and geomorphology: Are improvements in data collection techniques transforming geomorphic science? *Geomorphology* 270 121-133. DOI: 10.1016/j.geomorph.2016.07.011
- [30] Alcalá-Reygosa J 2019 Rock glaciers of the mountains of Mexico; a review of current knowledge and paleoclimatic implications. *Journal of South American Earth Sciences* 96 102321. DOI: 10.1016/j.jsames.2019.102321.
- [31] Palacios D, Stokes C R, Phillips F M, Clague J J, Alcalá-Reygosa J, Andrés N, Angel I, Blard P H, Briner J P, Hall B L, Dahms D, Hein A S, Jomelli V, Mark B G, Martini M A, Moreno P, Riedel J, Sagredo E, Stansell N D, Vázquez-Selem L, Vuille M, Ward D J 2020 The

- deglaciation of the Americas during the Last Glacial Termination. *Earth-Science Reviews* 203 103-113. DOI: <https://doi.org/10.1016/j.earscirev.2020.103113>
- [32] Blahut J, Mitrovic-Woodell I, Baron I, Rene M, Rowberry M, Blard PH, Hartvich F, Balek J, Meletlidis S 2020 Volcanic edifice slip events recorded on the fault plane of the San Andres Landslide, El Hierro, Canary Islands. *Tectonophysics*, 776: 228317. DOI: 10.1016/j.tecto.2019.228317
- [33] Nesje A, McCarroll D, Dahl S O 1994 Degree of rock surface weathering as an indicator of ice-sheet thickness along an east-west transect across southern Norway. *Journal of Quaternary Science* 9 337-347
- [34] Clark R, Wilson P 2004 A rock avalanche deposit in Burtness Comb, Lake District, northwest England. *Geological Journal* 39 3-4 419-430. DOI: 10.1002/gj.965.
- [35] Aa R A, Sjastad J, Sønstegaard E, Blikra L H 2007 Chronology of Holocene rockavalanche deposits based on Schmidt-hammer relative dating and dust stratigraphy in nearby bog deposits, Vora, inner Nordfjord, Norway. *The Holocene* 17 955-964. DOI: 10.1177/0959683607082411
- [36] Decaulne A, Saemundsson D, Jonsson H P, Sandberg O 2007 Changes in deposition on a colluvial fan during the Upper Holocene in the Tindastoll Mountain, Skagafjorthur District, north Iceland: Preliminary results. *Geografiska Annaler Series A-Physical Geography*, 89A 1 51-63. DOI: 10.1111/j.1468-0459.2007.00307.x
- [37] Ietto F, Donato F F 2007 Recent reverse faults and landslides in granitoid weathered profiles, Serre mountains (southern Calabria, Italy). *Geomorphology*, 87 3 196-206. DOI: 10.1016/j.geomorph.2006.03.042
- [38] Del Potro R, Hurlimann M 2008 Geotechnical classification and characterisation of materials for stability analyses of large volcanic slopes. *Engineering Geology*, 98 1-2: 1-17. DOI: 10.1016/j.enggeo.2007.11.007
- [39] Klimes J, Vilimek V, Omelka M 2009 Implications of geomorphological research for recent and prehistoric avalanches and related hazards at Huascarán, Peru. *Natural Hazards*, 50 1 193-209. DOI: 10.1007/s11069-008-9330-7
- [40] Wilson P 2009 Storurdi: a late holocene rock-slope failure (sturzstrom) in the jotunheimen, southern norway. *Geografiska Annaler: Series A, Physical Geography*, 91A 1 47-58. DOI: 10.1111/j.1468-0459.2009.00352.x
- [41] Owen G, Hiemstra J F, Matthews J A, McEwen L J 2010 Landslide-glacier interaction in a neoparaglacial setting at tverrybytnede, jotunheimen, southern norway. *Geografiska Annaler: Series A, Physical Geography*, 92A,4: 421-436. DOI: 10.1111/j.1468-0459.2010.00405.x
- [42] Burda J, Vesely M, Rehor M, Vilimek V 2018 Reconstruction of a large runout landslide in the Krun, hory Mts. (Czech Republic). *Landslides*, 15,3: 423-437. DOI: 10.1007/s10346-017-0881-0
- [43] Yepes J, Lomoschitz A 2008 Landslide deposits of the Fataga ravine (Gran Canaria Island). *Geo-Temas*, 10: 231-234. Proceedings of the VII Congreso Geológico de España. Las Palmas de Gran Canaria.
- [44] Yepes J, Lomoschitz A 2009 Caracterización geomorfológica del alud de rocas de Arteara. Proceedings of the VII Simposio Nacional sobre Taludes y Laderas Inestables. Eds. E. Alonso, J. Corominas y M. Hürlimann. 1 351-362. Barcelona.
- [45] Yepes J, Lomoschitz A 2010 Geomorphology of the Arteara Holocene rock-avalanche deposit, Gran Canaria Island. *Geophysical Research Abstracts*, 12: EGU2010-12017
- [46] Rodríguez-Peces M J, Yepes J, Martín-Nicolau E 2012 Geotechnical parameters of the volcanic rocks related to the Arteara rock avalanche (Gran Canaria, Canary Islands). *Geo-Temas*, 13: 3160-3164. Proceedings of the VIII Congreso Geológico de España. Oviedo
- [47] Rodríguez-Peces M J, Yepes J, Martín-Nicolau E 2013 Geotechnical features of the volcanic rocks related to the Arteara rock avalanche in Gran Canaria (Canary Islands, Spain). In *Landslide Science and Practice: Spatial Analysis and Modelling*, Eds. C. Margottini, P.

Canuti, K. Sassa. 3 111-117

- [48] Santana M, Estaire J, Yepes J 2014 Geotechnical characterization of rocky materials from Arteara rock avalanche (Gran Canaria). In *Rock Engineering and Rock Mechanics: Structures in and on Rock Masses* Eds. Alejano, Perucho, Olalla y Jiménez. 1(76) 479-484